AIAA JOURNAL
Vol. 30, No. 10, October 1992

Vortical Flow Computations on a Flexible Blended Wing-Body Configuration

Guru P. Guruswamy*
NASA Ames Research Center, Moffett Field, California 94035

Flows over blended wing-body configurations are often dominated by vortices. The unsteady aerodynamic forces due to such flows can couple with the elastic forces of the wing and lead to aeroelastic oscillations. Such aeroelastic oscillations can impair the performance of an aircraft. To study this phenomenon, it is necessary to account for structural properties of the configuration, and solve the aerodynamic and aeroelastic equations of motion simultaneously. In this work, the flow is modeled using the Navier-Stokes equations coupled with the aeroelastic equations of motion. Computations are made for a blended wing-body configuration at flow conditions dominated by vortices and separation. The computed results are validated with the available experimental data. Almost sustained aeroelastic oscillations observed in the wind tunnel are successfully simulated for $M_\infty = 0.975$, $\alpha \approx 8.0$ deg, and a frequency of about 2 Hz.

Nomenclature

C_p	= coefficient of pressure
$\{d\}$	= displacement vector
E, F, G, Q	= flux vectors in Cartesian coordinates
$[M], [D], [K]$	= modal mass, damping, and stiffness matrices, respectively
$\{q\}$	= generalized displacement vector
Re_c	= Reynolds number based on the root chord
U	= flight velocity
u, v, w	= velocity components in x, y, and z directions, respectively
$\{Z\}$	= generalized force vector
x, y, z	= Cartesian coordinates
α	= rigid angle of attack
α_e	= elastic angle of attack
Δ	= difference between upper and lower surface pressures
ξ, η, ζ	= general curvilinear coordinates
τ	= nondimensional time
$[\phi]$	= modal displacement matrix
$(\hat{})$	= quantities in generalized coordinate system
$(\dot{})$	= first derivative with respect to time
$(\ddot{})$	= second derivative with respect to time

Subscript

∞	= freestream quantities

Introduction

FLOWS with vortices play an important role in the development of aircraft. In general, strong vortices form on aircraft at large angles of attack. For aircraft with highly swept wings, strong vortices can even form on the wings at moderate angles of attack. The formation of vortices changes the aerodynamic load distribution on a wing. Vortices formed on aircraft have been known to cause several undesirable phenomena such as wing rock for rigid delta wings[1] and aeroelastic oscillations for highly swept flexible wings.[2] Such phenomena can severely impair the performance of an aircraft. On the other hand, vortical flows can also play a positive role in the design of an aircraft. Vortical flows associated with rapid, unsteady motions can increase the unsteady lift, which can be used for maneuvering the aircraft.[3]

To date, most of the calculations for wings with vortical flows have been restricted to steady and unsteady computations on rigid wings. However, to accurately compute such flows, it is necessary to account for the wing's flexibility. The aeroelastic deformation resulting from this flexibility can considerably change the nature of the flow. Strong interactions between the vortical flows and the structures can lead to sustained aeroelastic oscillations for highly swept wings.[2] Also, it is necessary to include the flexibility for proper correlations of computed data with experiments, particularly with those obtained from flight tests. Recent efforts have been made to include the flexibility of wings in the calculations.[4] To compute the flows accurately, it is necessary to include both aerodynamic and structural effects of the body. In this work, the flow is modeled using the Navier-Stokes equations coupled with the aeroelastic equations of motion for blended wing-body configurations. The Navier-Stokes equations are required to accurately model the viscous effects on vortical flows.

The computer code developed for computing the unsteady aerodynamics and aeroelasticity of aircraft by using the Navier-Stokes equations is referred to as ENSAERO.[5] The capability of the code to compute aeroelastic responses by simultaneously integrating the Navier-Stokes equations and the modal structural equations of motion, using aeroelastically adaptive dynamic grids, has been demonstrated.[5] The flow is solved by time-accurate, finite difference schemes based on the Beam-Warming algorithm. Recently, a new streamwise upwind scheme has also been incorporated in the code.[6]

In this work, the capability of the code is extended to model the Navier-Stokes equations with the Baldwin-Lomax turbulence model for blended wing-body configurations. It is noted here that turbulence models, such as the quasisteady model of Baldwin-Lomax currently used for the Navier-Stokes equations, still require several improvements, particularly for computing self-induced unsteady flows. In this paper, computations are made for cases where the flow unsteadiness is initiated by an initial disturbance given to the structure. The quasisteady turbulence model is assumed to be adequate for

Received April 4, 1991; presented as Paper 91-1013 at the AIAA/ASME/ASCE/AHS 32nd Structures, Structural Dynamics, and Materials Conference, April 8-10, 1991, Baltimore, MD; revision received March 12, 1992; accepted for publication March 16, 1992.

*Research Scientist. Associate Fellow AIAA.

this problem, but further careful investigation is needed in using existing turbulence models for other similar cases.

In this paper, computations are presented for vortical flow conditions about a flexible blended wing-body configuration and the results are compared with the available experiments. The formation of vortices and their effects on the aeroelastic responses are demonstrated.

Governing Aerodynamic Equations

The strong conservation law form of the Navier-Stokes equations is used for shock-capturing purposes. The thin-layer version of the equations in generalized coordinates can be written as[7]

$$\partial_\tau \hat{Q} + \partial_\xi \hat{E} + \partial_\eta \hat{F} + \partial_\zeta \hat{G} = Re^{-1}\partial_\zeta \hat{S} \tag{1}$$

where $\hat{Q}$, $\hat{E}$, $\hat{F}$, $\hat{G}$, and $\hat{S}$, are flux vectors in generalized coordinates. The following transformations are used in deriving Eq. (1).

$$\tau = t \tag{2a}$$

$$\xi = \xi(x,y,z,t) \tag{2b}$$

$$\eta = \eta(x,y,z,t) \tag{2c}$$

$$\zeta = \zeta(x,y,z,t) \tag{2d}$$

It should be emphasized that the thin-layer approximation is valid only for high-Reynolds-number flows and very large turbulent eddy viscosities invalidate the model.

To solve Eq. (1), ENSAERO has time-accurate methods based on both central difference and upwind schemes.[6] In this paper, the central difference scheme based on the implicit approximate factorization algorithm of Beam and Warming[8] with modifications by Pulliam and Chaussee[9] for diagonalization is used. This scheme is first-order accurate in time.

The diagonal algorithm is fully implicit for the Euler equations. For the Navier-Stokes equations the diagonal algorithm works as an explicit scheme since viscous terms on the right-hand side of Eq. (1) are treated explicitly. The diagonal algorithm is first-order accurate in time for both Euler and Navier-Stokes equations. Numerical exercises conducted during this work and in previous work reported in Ref. 5 showed that the timestep size required to solve Eq. (1) is limited by accuracy rather than stability considerations. Therefore, the explicitness of the diagonal algorithm does not influence the computational efficiency when solving the Navier-Stokes equations.

For turbulent flow, the coefficient of viscosity appearing in Eq. (1) is modeled using the Baldwin-Lomax algebraic eddy-viscosity model.[10] This isotropic model is used primarily because it is computationally efficient. All viscous computations presented in this paper assume fully turbulent flow. This approximation is consistent with the high-Reynolds-number assumption. Because of the vortex-dominated flow structures of the blended wing-body configuration, a modification to the original Baldwin-Lomax model is required. For this study, the Degani-Schiff modification[11] to the original model for treating vortical flows is used. However, as noted earlier, the Baldwin-Lomax turbulence model is based on quasisteady assumptions. Therefore it may be inadequate to model self-induced flow unsteadiness.

Aeroelastic Equations of Motion

The governing aeroelastic equations of motion of a flexible blended wing-body configuration are obtained by using the Rayleigh-Ritz method. In this method, the resulting aeroelastic displacements at any time are expressed as a function of a finite set of assumed modes. The contribution of each assumed mode to the total motion is derived by the Lagrange's equation. Furthermore, it is assumed that the deformation of the continuous wing structure can be represented by deflections at a set of discrete points. This assumption facilitates the use of discrete structural data, such as the modal vector, the modal stiffness matrix, and the modal mass matrix. These can be generated from a finite element analysis or from experimental influence coefficient measurements. In this study, the finite element method is employed to obtain the modal data.

It is assumed that the deformed shape of the wing can be represented by a set of discrete displacements at selected nodes. From the modal analysis, the displacement vector $\{d\}$ can be expressed as

$$\{d\} = [\phi]\{q\} \tag{3}$$

where $[\phi]$ is the modal matrix and $\{q\}$ is the generalized displacement vector. The final matrix form of the aeroelastic equations of motion is

$$[M]\{\ddot{q}\} + [G]\{\dot{q}\} + [K]\{q\} = \{Z\} \tag{4}$$

where $[M]$, $[G]$, and $[K]$ are modal mass, damping, and stiffness matrices, respectively. $\{Z\}$ is the aerodynamic force vector defined as $\frac{1}{2}\rho U_\infty^2[\phi]^T[A]\{\Delta C_p\}$ and $[A]$ is the diagonal area matrix of the aerodynamic control points.

The aeroelastic equation of motion, Eq. (4), is solved by a numerical integration technique based on the linear acceleration method.[12]

Aeroelastic Configuration Adaptive Grids

One of the major difficulties in using the Navier-Stokes equations for computational aerodynamics lies in the area of grid generation. For steady flows, the advanced techniques such as zonal grids[13] are currently being used. However, grid-generation techniques for aeroelastic calculations, which involve moving components, are still in the early stages of development. In Ref. 5, aeroelastic configuration adaptive dynamic grids were successfully used for computing time-accurate aeroelastic responses of wings. In this work, a similar technique that is suitable for accurately simulating vortical flows on flexible wing-body configurations is used. The grid is designed such that the formation of vortices and their movement on the wing can be captured. The grid is generated at every timestep based on the aeroelastic position of the wing. Details of this grid-generation technique are given in Ref. 5.

The diagonal algorithm used in the present study computes time-accurate solutions in a geometrically nonconservative fashion. Geometric conservativeness can improve the accuracy of the results for moving grids. However, earlier studies have shown that the inclusion of geometric conservativeness has little effect on the solutions associated with the moving grids.[6] The timesteps used for calculations with moving grids are typically small enough that the error from geometric nonconservativeness is negligible for most practical purposes. The validation of computed results with experiments reported in Refs. 4 and 5 further support the use of the diagonal scheme for computations associated with moving grids. To maintain the efficiency and robustness of the diagonal scheme, the present time-accurate computations are made without geometric conservativeness. Computational efficiency and robustness of the solution method are important for computationally intensive aeroelastic calculations with configuration-adaptive grids.

Results

To validate the present development, computations were made for a blended wing-body configuration shown in Fig. 1. The root of the wing is located at the 46% wing-body semispan section measured from the centerline of the configuration. The flexibility of the configuration starts from the wing root. The wing has a high sweep angle of 67.5 deg measured at the elastic axis. For this configuration, aerodynamic and

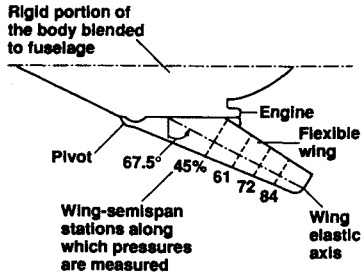

Fig. 1 Wind-tunnel model of the blended wing-body configuration.

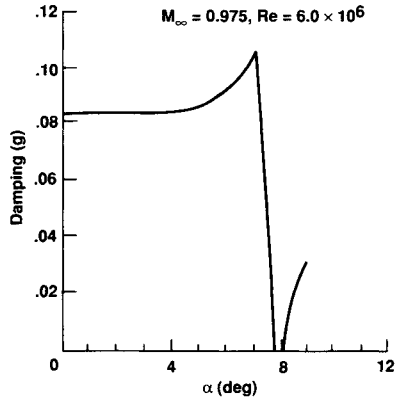

Fig. 2 Plot of damping vs angle of attack taken from wind-tunnel test.

aeroelastic experimental data are given in Ref. 2. For this sweep angle, measurements were made at various flow conditions in order to investigate the effects of vortical flows on the aeroelastic responses of the wing.

In Fig. 2, a plot of aeroelastic damping vs the angle of attack taken from Ref. 2 shows that the configuration undergoes limit cycle oscillations at $M_\infty = 0.975$, $Re_c = 6.0 \times 10^6$, and $\alpha \approx 8.0$ deg. At other angles of attack the configuration is dynamically stable. It was observed in the experiment that the configuration experienced oscillations predominantly in the first bending mode. Hence, this oscillation is not associated with the conventional bending-torsion flutter. The wind-tunnel tests did not provide the reasons for these aeroelastic oscillations. A detailed investigation,[14] based on the computations made using an inviscid transonic small perturbation code and experiments reported in Ref. 2, led to the possibilities of aeroelastic oscillations associated with vortices. The results in Ref. 14 strongly ruled out any possibilities of shock-induced oscillations and led to the possibilities of vortex-induced oscillations. However, it could not be completely confirmed since the transonic small perturbation theory cannot model vortices. The wind-tunnel results also indicated flow separations when the wing underwent aeroelastic oscillations. This phenomenon is investigated in this paper by using the Navier-Stokes results with a turbulence model.

In this paper, computations are presented at two flow conditions for which detailed data were available to the author from the wind-tunnel tests. First, computations are shown at $M_\infty = 0.805$, $Re_c = 7.5 \times 10^6$, and $\alpha = 10.5$ deg at which there are no aeroelastic oscillations. This case is selected to validate the computational model of the configuration by comparing the static aeroelastic data with the wind-tunnel test. Next, computations are shown at $M_\infty = 0.975$, $Re_c = 6.0 \times 10^6$, and for $\alpha = 0.0$, 8.0, and 12.0 deg. These cases are selected since at $\alpha \approx 8.0$ deg (see Fig. 2) the configuration experienced aeroelastic oscillations.

The body portion of this configuration is rigid and the wing portion is flexible. The modal data required for the aeroelastic analysis is computed by the finite element method. Figure 3 shows the mode shapes and frequencies of the first six normal modes for the current configuration. This modal data compares well with the measured data.[2]

The wing-body configuration shown in Fig. 1 is modeled using a C-H type grid of size $151 \times 40 \times 40$. Figure 4 shows the symmetry plane and configuration upper surface of the grid. Earlier studies using this grid showed that it is adequate to accurately compute the flows with vortices and separations up to $\alpha = 12$ deg for a highly swept wing.[15] To further validate the adequacy of this grid for computations using the Navier-Stokes equations, static aeroelastic computations were made at several flow conditions and results were compared with the experiment. Figure 5 shows the comparison between the computed and measured steady pressures at $M_\infty = 0.805$, $Re_c = 7.5 \times 10^6$, and $\alpha = 10.5$ deg. The results are plotted for four sections which are normal to the elastic axes located along the 25% chord line. The comparisons are favorable for all span stations. The discrepancies near the trailing edge of the 84% semispan station are due to the simplifications made in modeling the tip. To simplify the grid, the tip chord is computationally modeled as parallel to the freestream whereas the actual tip is at an angle to the freestream. Figure 5 shows that the flow is dominated by the presence of a strong vortex on the wing and the flow is separated near the tip. This can also be seen in the density contours plotted at four span stations in Fig. 6 on the aeroelastically deformed wing. The presence of the vortex on the wing can be seen at 50% and 75% wing semispan stations in Fig. 6. The wing tip deflected by about 5% of the root chord due to aerodynamic loads. The same order of deflection was observed in the wind-tunnel tests.[2]

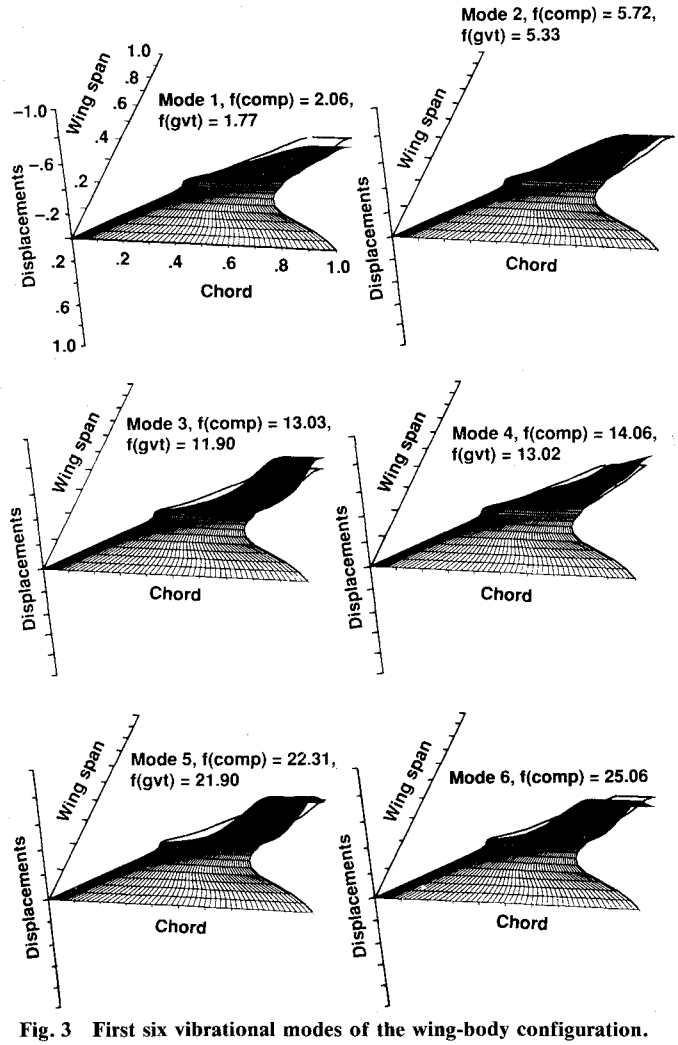

Fig. 3 First six vibrational modes of the wing-body configuration.

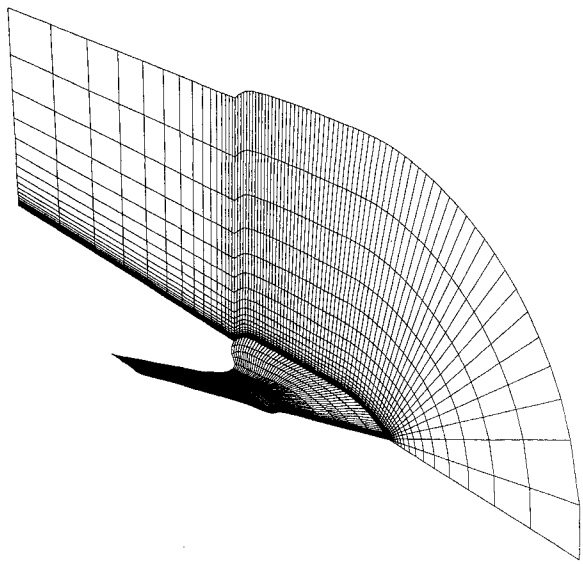

Fig. 4 A portion of the physical grid (151 × 40 × 40) around the surface.

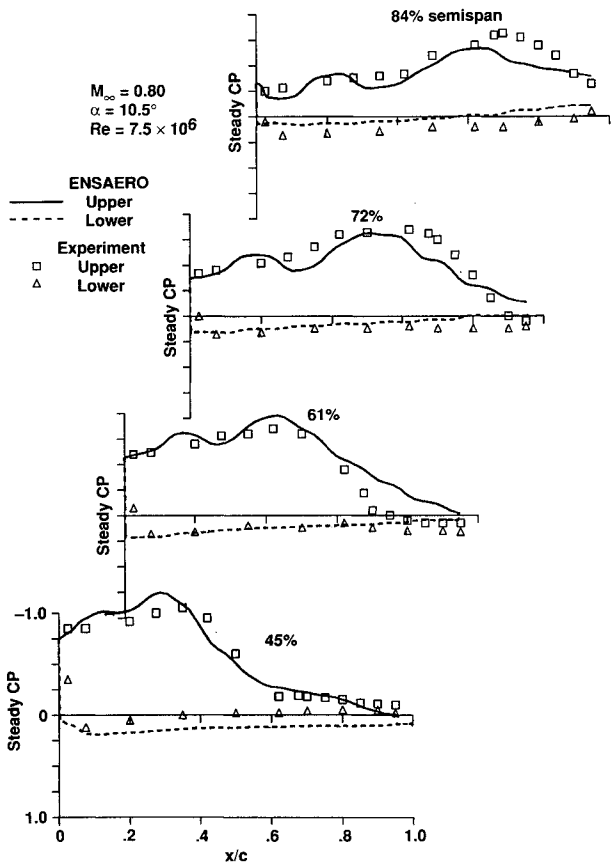

Fig. 5 Comparison of steady pressures with the experiment.

These calculations confirm the validity of the grid and aeroelastic modeling of the configuration.

By using the normal modal data shown in Fig. 3, aeroelastic responses were computed by simultaneously integrating the flow equation [Eq. (1)] and the aeroelastic equation [Eq. (4)] in ENSAERO. Freestream conditions are used as initial conditions for the flow. The wing is started from a rigid steady-state position. Aeroelastic responses are computed at $M_\infty = 0.975$, $Re_c = 6.0 \times 10^6$, and angles of attack of 0.0, 8.0, and 12.0 deg. The dynamic pressure is set to 1.60 psi, which corresponds to that used in the wind tunnel to simulate flight conditions at an altitude of 32,000 ft. All aeroelastic oscillations are initiated by giving a small initial disturbance to the wing by setting the initial value of the generalized displace-

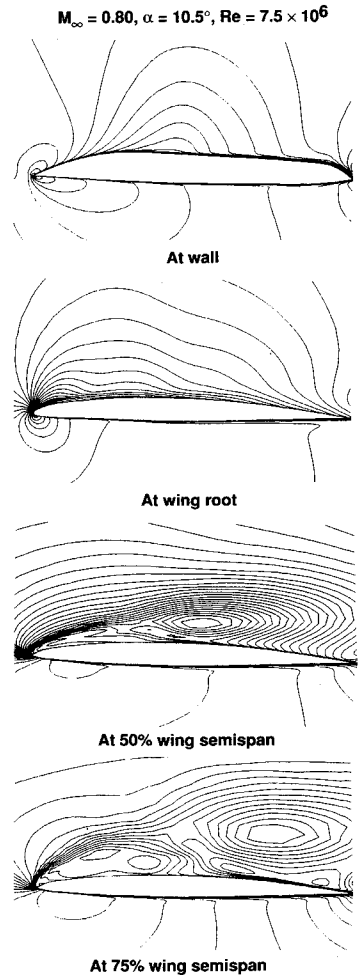

Fig. 6 Density contours on the aeroelastically deformed configuration.

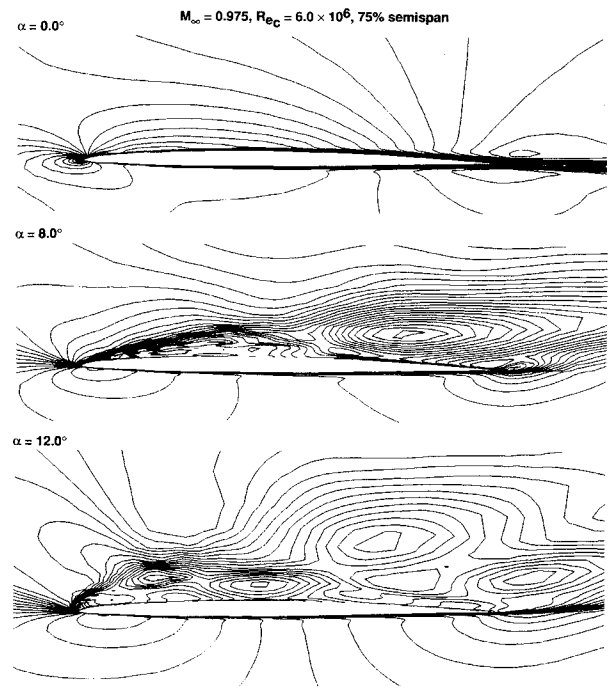

Fig. 7 Density contours at angles of attack of 0.0, 8.0, and 12.0 deg.

ment $q(1)$ to 0.01 and the remaining displacements to zero.

Steady-state computations are presented at three angles of attack of 0.0, 8.0, and 12.0 deg. The corresponding density contours are shown in Fig. 7. From Fig. 7 it can be seen that vortices on the wing are present at angles of attack of 8.0 and 12.0 deg. The flow begins to separate at $\alpha = 8.0$ deg and is fully separated at $\alpha = 12.0$ deg. As a result of flow separation, the vortex near the tip is lifted off the wing for $\alpha = 12.0$ deg. This leads to lower sectional lift near the tip.

Aeroelastic computations are started from the steady-state converged solution. Aeroelastic equations of motion are integrated simultaneously with the Navier-Stokes equations. A nondimensional timestep size that corresponds to a physical time of 0.00024 s per timestep is used. From numerical experiments, it is found that this timestep size is adequate to accurately compute the time responses. ENSAERO, which runs at a speed of 150 MFLOPS, requires 4.5 s of CPU time per timestep on a Cray YMP using a single processor for current 241,600 grid points. For all angles of attack, the equations of motion are integrated for 12,500 timesteps, which corresponds to a physical time of 3.0 s. Starting from the converged steady-state solution, which requires 5 h of CPU time, each aeroelastic response requires about 16 h of CPU time.

At $\alpha = 0.0$ deg the flow is fully attached throughout the aeroelastic response. For $\alpha = 8.0$ and 12.0 deg, the flow stayed separated throughout the aeroelastic responses. The present computations do not involve flow reattachment cases.

Figure 8 shows the unsteady sectional lift coefficients for three angles of attack at the root; 25%, 50%, and 75% of wing semispan stations. Since the wing is rigidly fixed to the root, fluctuations in the lift near the root are small. The

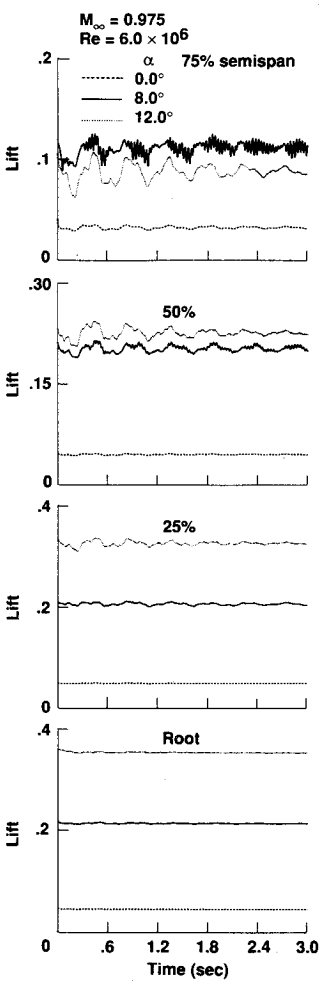

Fig. 8 Unsteady lift responses at angles of attack of 0.0, 8.0, and 12.0 deg.

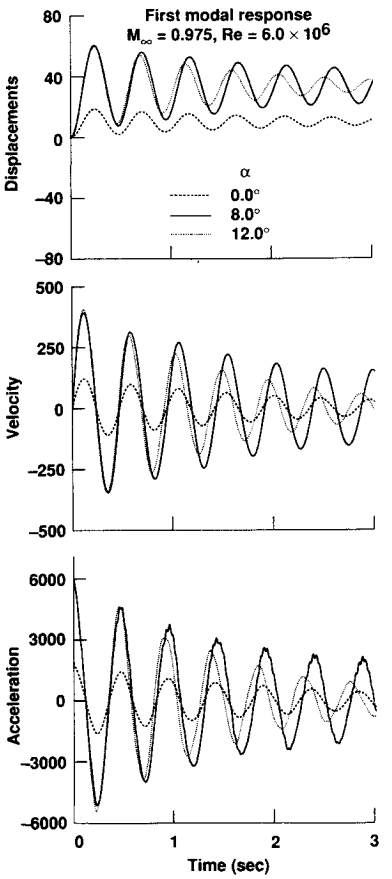

Fig. 9 Modal responses at angles of attack of 0.0, 8.0, and 12.0 deg.

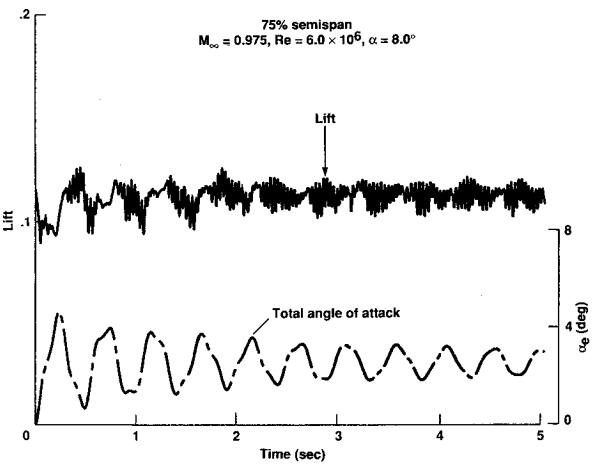

Fig. 10 Lift and elastic angle response at 8.0-deg angle of attack.

fluctuations in lift increase towards the tip because of the wing's flexibility. These fluctuations have two main components, one due to the aeroelastic oscillations of the wing and the other due to the unsteadiness in the flow. It is noted here that the flow unsteadiness is initiated by an initial disturbance given to the structure. The fluctuations for $\alpha = 0.0$ deg is only due the aeroelastic oscillations. For angles of attack of 8.0 and 12.0 deg, the fluctuations contain components from both aeroelastic oscillations and flow unsteadiness. The contribution of flow unsteadiness to the fluctuations is greater for the $\alpha = 8.0$ deg case than for $\alpha = 12.0$ deg case. This can be seen in Fig. 8, particularly at the 75% semispan station. It is also noticed that the magnitude of the lift for $\alpha = 12.0$ deg is smaller than that for $\alpha = 8.0$ deg at the 75% semispan station. The reduction in both the magnitude and unsteadiness of the

lift at 12.0 deg is due to a weaker interaction between the wing movement and vortex. One possible reason for such weaker interaction at $\alpha = 12.0$ deg is the presence of a thicker boundary layer on which the vortex rides during the oscillations. The lift reduction can also come from the reduction in the local angle of attack due to bending. However, by studying the structural responses it is found that the effect of the changes in the local angle of attack is negligible when compared to the effect of the changes in the flow structure.

Figure 9 shows the responses of the first mode for all three angles of attack. The response at $\alpha = 8.0$ deg has less damping than the responses at $\alpha = 0.0$ and 12.0 deg. At $\alpha = 8.0$ deg, the flow unsteadiness has strongly influenced the aeroelastic responses. This can be seen in the acceleration response in Fig. 9. The high-frequency oscillations associated with the flow unsteadiness is present only for $\alpha = 8.0$ deg. It is also observed that the damping for $\alpha = 8.0$ deg is approaching zero as time reaches 3.0 s.

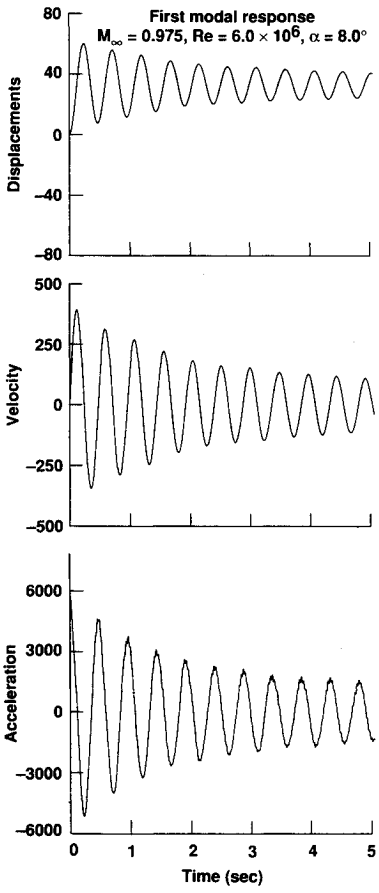

Fig. 11 First modal response at 8.0-deg angle of attack.

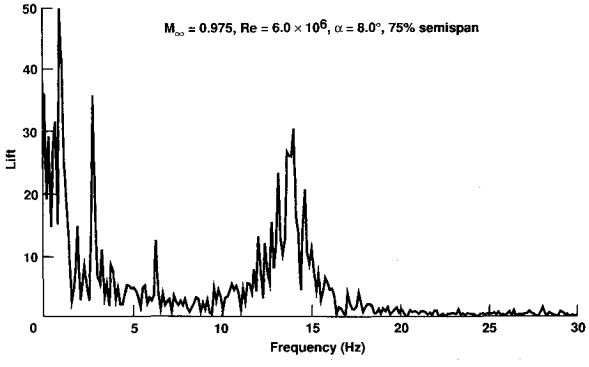

Fig. 12 Fourier analysis results of sectional lift at 8.0-deg angle of attack.

To further confirm the low-damping phenomenon of the response at $\alpha = 8.0$ deg, aeroelastic computations were continued for this case up to 5 s of physical time. The lift and corresponding elastic angle-of-attack responses are shown in Fig. 10. From both responses, it can be seen that the configuration has almost reached a limit cycle oscillation before 5.0 s. This can be further confirmed by the response of the first mode shown in Fig. 11. All of the other five modal responses show similar behavior. Hence, it is confirmed that the configuration approaches limit cycle oscillations near $\alpha = 8.0$ deg and predominantly oscillates in its first bending mode. These results are confirmed by the wind-tunnel tests[2] as seen in Fig. 2.

A Fourier analysis is conducted on the lift responses to further investigate the cause for these aeroelastic oscillations. Typical results from Fourier analysis are shown for the 75% semispan section in Fig. 12. This plot shows that most of the contribution from flow unsteadiness is concentrated near the low frequencies around 2 Hz and high frequencies around 14 Hz. The energy contribution of the flow at low frequencies near 2 Hz has lead to almost sustained aeroelastic oscillations. It is noted that the wing oscillated in the wind tunnel at a frequency of about 2 Hz.

Because of the lack of detailed flow measurements, the wind-tunnel results cannot provide the complete explanation for the phenomenon of angle-of-attack dependent aeroelastic oscillations. Also, conventional flutter analysis cannot provide an explanation since it does not account for vortices and flow separations. Based on the present computations, the following explanation can be given for the phenomenon. At $\alpha = 0.0$ deg, the flow is fully attached and free from vortices. Based on the classical flutter theory, the swept wing is stable at these conditions. At $\alpha = 8.0$ deg, the flow is dominated by the presence of a strong vortex on the wing with small amounts of flow separation near the tip. The presence of a strong vortex leads to higher suction pressure on the wing as seen in Fig. 7. At these conditions, there is a strong interaction between the structure and the flow. Since the flow is very sensitive to any disturbance, it is highly unsteady. As a result, any small disturbance leads to almost sustained aeroelastic oscillations as seen in Figs. 10 and 11. At $\alpha = 12.0$ deg, the flow is fully separated and the boundary layer becomes thick as seen in Fig. 7. As a result, there is a weak interaction between the structure and flow and any disturbance quickly damps out.

Conclusions

In this paper, a computational procedure for computing the unsteady flows associated with vortices on flexible blended wing-body configurations has been presented. The procedure is based on a time-accurate computational method suitable for aeroelastically adaptive dynamic grids. To accurately model the viscous effects on the vortices, the flow is modeled using the Navier-Stokes equations. The flow equations are coupled with the structural equations to account for the flexibility. Based on this work, the following can be concluded:

1) The Navier-Stokes results are in good agreement with the static aeroelastic pressure measurements.

2) The computed results exhibit almost sustained oscillations previously seen in the wind tunnel. Earlier inviscid results could not show this phenomenon.

3) The unsteady vortex interaction can cause aeroelastic oscillations.

4) The present work does not include validation of unsteady aerodynamic data since no such data is currently available from the measurements. The preceding conclusions are based on the validation of the code ENSAERO for unsteady flows in the earlier work and also the validation of static and dynamic aeroelastic response results in this work.

5) Experiments that generate a detailed data base for both aerodynamic and aeroelastic validation are needed.

6) The use of quasisteady turbulence models may impose a severe limitation to the successful extension of this approach to the computation of self-induced flow unsteadiness. There-

fore, future efforts need to concentrate on modifying current turbulence models.

7) The geometric and structural data are too large to present within the page limitations of this paper. However, those who are interested can obtain the data through NASA by writing a letter to the author.

Acknowledgment

The author appreciates the help from Hiroshi Ide of Rockwell International in supplying the experimental data.

References

[1]Nguyen, L. T., Yip, L. P., and Chambers, J. R., "Self-Induced Wing Rock Oscillations of Slender Delta Wings," AIAA Paper 81-1883, Albuquerque, NM, Aug. 1981.

[2]Dobbs, S. K., and Miller, G. D., "Self-Induced Oscillation Wind Tunnel Test of a Variable Sweep Wing," AIAA Paper 85-0739, Orlando, FL, April 1985.

[3]Mabey, D. G., "On the Prospects for Increasing Dynamic Lift," *Aeronautical Journal Royal Aeronautical Society,* March 1988, pp. 95-105.

[4]Guruswamy, G. P., "Unsteady Aerodynamic and Aeroelastic Calculations of Wings Using Euler Equations," *AIAA Journal,* Vol. 28, No. 3, 1990, pp. 461-469.

[5]Guruswamy, G. P., "Navier-Stokes Computations on Swept-Tapered Wings, Including Flexibility," AIAA Paper 90-1152, Long Beach, CA, April 1989.

[6]Obayashi, S., Guruswamy, G. P., and Goorjian, P. M., "Streamwise Upwind Algorithm for Computing Unsteady Transonic Flows Past Oscillating Wings," *AIAA Journal,* Vol. 29, No. 10, 1991, pp. 1668-1677.

[7]Peyret, R., and Viviand, H., "Computation of Viscous Compressible Flows Based on Navier-Stokes Equations," AGARD AG-212, Sept. 1975.

[8]Beam, R., and Warming, R. F., "An Implicit Finite-Difference Algorithm for Hyperbolic Systems in Conservation Law Form," *Journal of Computational Physics,* Vol. 22, No. 9, 1976, pp. 87-110.

[9]Pulliam, T. H., and Chaussee, D. S., "A Diagonal Form of an Implicit Approximate Factorization Algorithm," *Journal of Computational Physics,* Vol. 39, No. 2, 1981, pp. 347-363.

[10]Baldwin, B. S., and Lomax, H., "Thin-Layer Approximation and Algebraic Model for Separated Turbulent Flows," AIAA Paper 78-257, Huntsville, AL, Jan. 1978.

[11]Degani, D., and Schiff, L. B., "Computation of Turbulent Supersonic Flows Around Pointed Bodies Having Cross Flow Separation," *Journal of Computational Physics,* Vol. 66, No. 1, 1986, pp. 173-196.

[12]Guruswamy, G., and Yang, T. Y., "Aeroelastic Time Response Analysis of Thin Airfoils by Transonic Code LTRAN2," *Computers and Fluids,* Vol. 9, No. 4, Dec. 1980, pp. 409-425.

[13]Flores, J., Chaderjian, N., and Sorenson, R., "The Numerical Simulation of Transonic Separated Flow About the Complete F-16A," AIAA Paper 88-2506, Willamsburg, VA, June 1988.

[14]Guruswamy, G. P., Goorjian, P. M., Ide, H., and Miller, G. D., "Transonic Aeroelastic Analysis of the B-1 Wing," *Journal of Aircraft,* Vol. 23, No. 7, 1986, pp. 547-553.

[15]Guruswamy, G., "ENSAERO—A Multidisciplinary Program for Fluid/Structural Interaction Studies of Aerospace Vehicles," *Computing Systems in Engineering,* Vol. 1, Nos. 2-4, 1990, pp. 237-256.